Materials Physics and Mechanics 39 (2018) 8-14 Received: November 1, 2017

ELECTRONIC AND OPTIC PROPERTIES OF TRANSITION METAL DICHALCOGENIDES (MoS_2, WSe_2) AND GRAPHENE HETEROSTRUCTURES

Maryia Baranava[1]*, Dzmitryi Hvazdouski[1], Viktor Stempitsky[1], Sviatlana Vauchok[1], Miroslav Najbuk[2]

[1]Belarusian State University of Informatics and Radioelectronics, Minsk, Belarus

[2]University of Bialystok, Poland

*e-mail: baranova@bsuir.by

Abstract. Double-layer heterostructures were studied. The energetic influence of the quasi-two-dimensional materials (MoS_2 and WSe_2) on the electrical properties of graphene was simulated. Electron density functional (DFT) implemented into VASP program was chosen to take into account van der Waals forces. Interlayer distances were determined for the systems studied by suitable electron density functional (DFT-D2). The distance is 3.50 Å for WSe_2/G and 3.45 Å for MoS_2/G respectively. Energy band structures were calculated; the influence of electric field on band structure being taken into account. A quantum-mechanical simulation was performed for determining dielectric permittivity, absorption coefficient, reflected index, Brewster angle and the critical angle.

Keywords: ab initio simulation, dichalcogenide, graphene, heterostructure, transition metal

1. Introdiction

Isolated graphene has a zero bandgap [1]. Two dimensional materials can be used for solving this problem. Graphene, having a zero band gap width, is a semimetal in the standard configuration in terms of conductivity [2]. This limits the possibility of its effective use as elements for designing micro- and nanoelectronic instrument structures. There are technological and constructive solutions that allow increasing the band gap width. In this case, graphene films become a semiconductor. In particular, for obtaining the band gap in graphene it is proposed to form:

- graphene nanoribbons, the band gap being created due to quantum limitations [2];
- structure from several layers (heterostructure) [3];
- use doped and strained graphene [4];
- influence by an external electric field on a multilayer graphene [5].

It is possible to control effectively the properties of graphene using dependence of its electronic characteristics on the energy influence of another material. Thus, graphene can be used as a structural element of a field-effect transistor.

Transition metal dichalcogenides (TMD) possess interesting properties that render them attractive for electronic applications similar to graphene. Molybdenum disulphide (MoS_2) is a semiconductor with a bulk band gap of about 1.2 eV. Its band gap can be modulated as a sample thickness decreases. The finite value of the band gap is the key advantage of molybdenite compared to graphene [6]. Combination of graphene and molybdenum in a

http://dx.doi.org/10.18720/MPM.3912018_2

heterostructure can lead to an interesting effect when the heterostructure components complement each other. In Ref. [7] the graphene/MoS_2/graphene heterostructures were studied. It was shown that such materials have better photon absorption properties, because of the enhanced light-matter interactions by the single-layer MoS_2.

Tungsten diselenide (WSe_2) is a layered TMD semiconductor having the band gap of about 1.2 eV [8]. The WSe_2 band structure transforms from indirect to direct gap in the monolayer limit [9]. Some graphene-based heterostructures retain high charge carrier mobility together with the appearance of semiconductor properties in graphene. This makes it possible to use such systems in many areas of nanoelectronics [10].

The purpose of this study is to investigate the electronic energy spectrum of graphene and transition metal chalcogenides being is a component of the heterostructures. The dependence of the electronic and optical properties of graphene and TMD on the energetic influence on each other is studied based on the results of quantum mechanical simulations.

2. Computational details

Our calculations are based on the density functional theory (DFT). The projector-augmented wave (PAW) potentials [11] and Perdew–Burke–Ernzerhof (PBE) functional [12] were used. The exchange–correlation potential was described through the local density approximation (LDA) [13]; Hubbard correction for 3d electrons of Mo and We (U = 5 eV) were employed. The cutoff energy of 480 eV and 5×5×1 *k*-point grids were determined by a fine grid of gamma-centered method [14] in the Brillouin zone. The valence electron configurations for Mo, S, We, Se and C were $4d^{10}5s^25p^2$, $3s^23p^4$, $5d^{10}6s^26p^2$ and $5s^25p^5$, respectively. The heterostructures were built from 3 unit cells of MoS_2 and 4 unit cells of C (MoS_2/G), as well as from 3 unit cells of WSe_2 and 4 unit cells of C (WSe_2/G). The atomic structures were relaxed until the forces on all unconstrained atoms were smaller than 0.01 eV/Å. The vacuum layer of 15 Å along z direction was constructed to eliminate the interaction with spurious replica images.

The investigated heterostructures are the systems in which strong covalent bonds in a plane form atomic layers that are held together by weak van der Waals forces. [15]. So at the first stage, for the adequate description of physical processes in the heterosystems, the electron density functional was chosen through the use of VASP (Vienna Ab-initio Simulation Package) software package [16]. DFT-D3 method of Grimme [17] was used to account for long-range van-der-Waals interaction between monolayers. Structural figures and charge density drawings were produced by VESTA package [18].

3. Results and Discussion

The supercell method was used to create heterostructures. At first the total energy optimization was performed for relaxation of unit cells of investigated materials. The unit cells of MoS_2 and graphene were replicated by 3 and 4 in each crystallographic direction, respectively. Just the same procedure took place for WSe_2/graphene heterostructure. The lattice mismatch of created heterostructures was about 3.01 percents for MoS_2/G and 1.15 percents for WSe_2/G. The shape and volume of supercells were considered to be unchangeable at self-consistent calculations. The calculated interlayer distances are 3.50 Å for WSe_2/G and 3.45 Å for MoS_2/G; they are shown in Figure 1.

Non-self-consistent calculations were carried out along the lines between the high symmetry points K-Γ-M-K of the first Brillouin zone. The energy dispersion of graphene sheet in heterostructure is similar to that of a pristine graphene, i.e. the zero band gap is conserved (Fig. 2).

Vertical electric field has little effect on the band gap WSe_2/G and MoS_2/G. The heterostructures have a direct band gap under influence E_{field} of 0.15 V/Å. Analysis of the

results showed that the vertical external electric field can regulate charge transfer between monolayers and graphene.

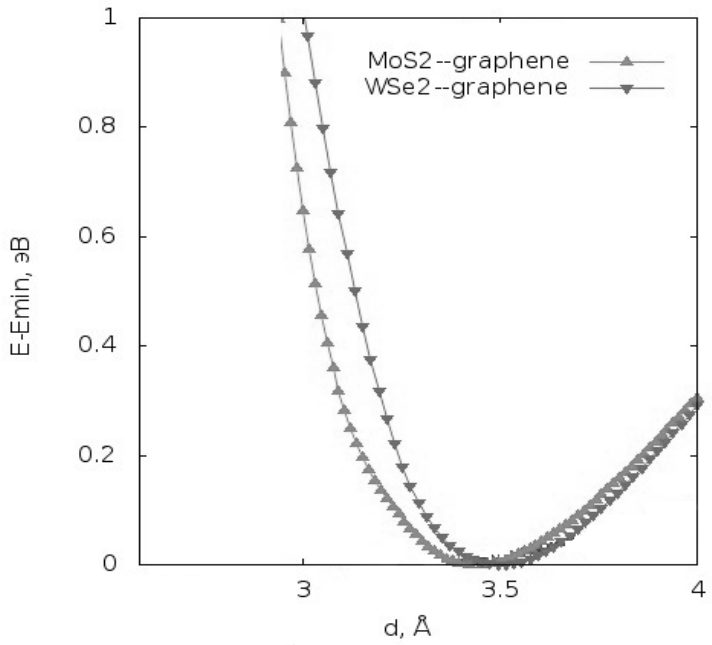

Fig. 1. Interlayer distance of heterostructures

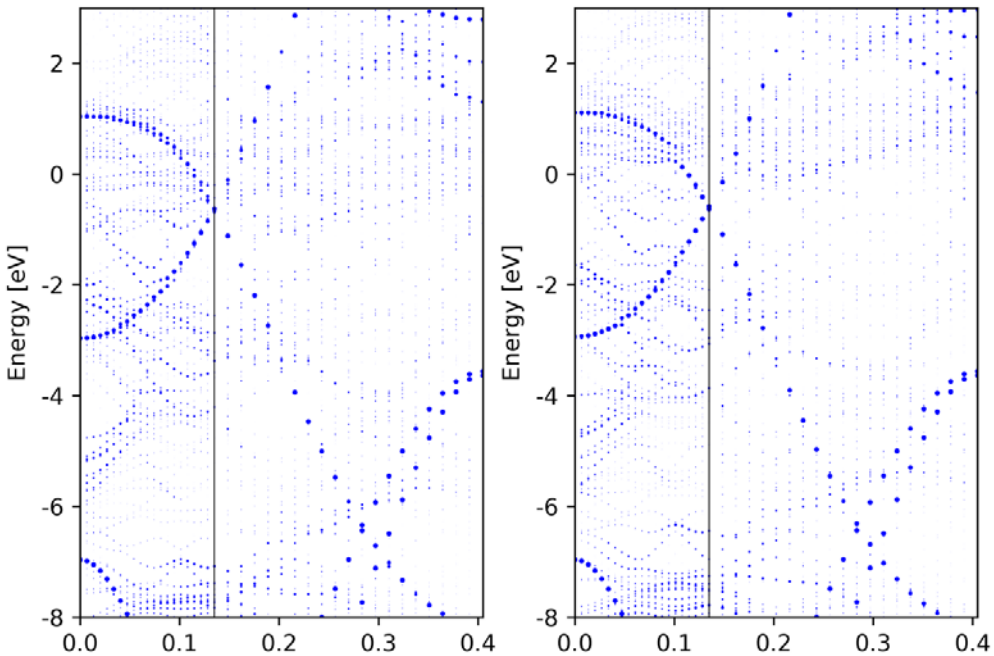

Fig. 2. Band structure of graphene on MoS_2 substarate (a) and on WSe_2 substarate (b)

A quantum-mechanical simulation was performed to determine the dielectric permittivity for a heterostructure consisting of graphene monolayer and MoS_2. The change in the real part of the dielectric permittivity indicates relaxation dispersion at frequencies corresponding to energy values from 0 to 3.5 eV; this type of dispersion is characteristic for a dipole and migration polarization mechanisms. Furthermore, the resonance dispersion occurs in the range from 3.5 to 9.5 eV, i.e. the ion and electronic polarization mechanisms are the

main (Fig. 3). The sharp difference between the real part of the dielectric permittivity in the range from 0 to 0.7 eV and the range from 1.0 to 8.0 eV is caused by the significant contribution of crystal lattice vibrations in comparison with the other components of the dielectric permittivity.

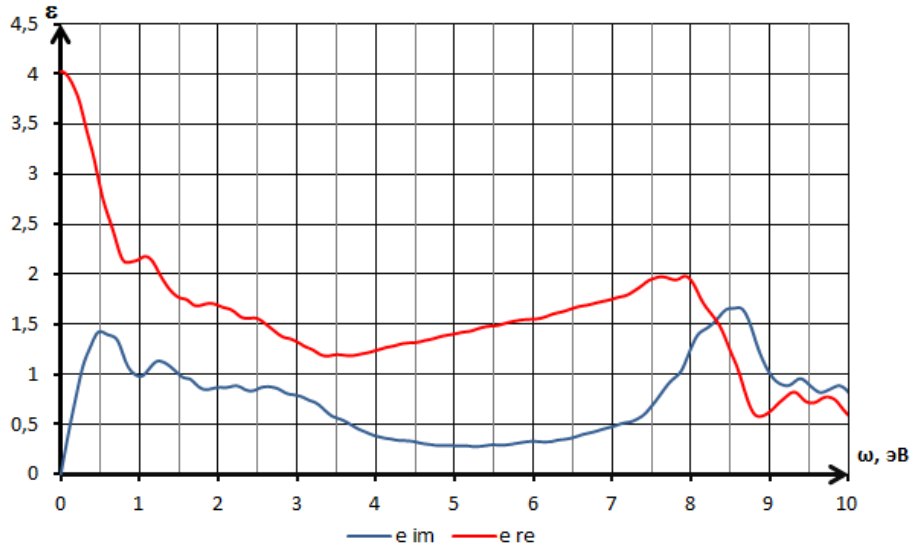

Fig. 3. Frequency dependence of the permittivity: imaginary (im) and real (re) constituents (MoS_2/ graphene)

Optic properties of the heterostructure were also simulated. Dispersion, having no sharp characteristic peaks on the dependence of absorption coefficient on frequency, was observed in the entire infrared and visible light range. The peak is observed at 8.5 eV. Consequently, the absorption increases only in the region of the far ultraviolet (Fig. 4). The heterostructure is optically transparent across the entire frequency spectrum. The refractive index in the visible light range is in the range from 1.12 to 1.5.

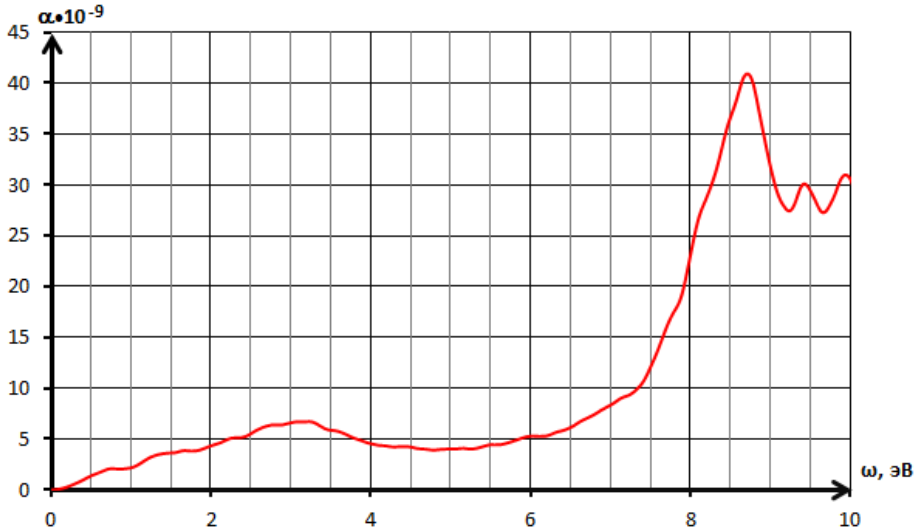

Fig. 4. Frequency dependence of the absorption coefficient (MoS_2/ graphene)

Analogous simulation was done for a heterostructure consisting of a graphene monolayer and WSe_2. The sharp difference between the real part of the dielectric permittivity in the range from 0 to 0.5 eV and the range from 0.5 to 8.0 eV is caused by the significant

contribution of crystal lattice vibrations in comparison with other components of the dielectric permittivity. The change in the real part of the dielectric permittivity points relaxation dispersion at frequencies corresponding to energy values from 0.5 to 7.0 eV; this type of dispersion being characteristic for a dipole and migration mechanisms of polarization. Furthermore, the resonance dispersion occurs in the range from 7.0 to 9.5 eV, i.e. the ion and electronic polarization mechanisms are the main ones (Fig. 5).

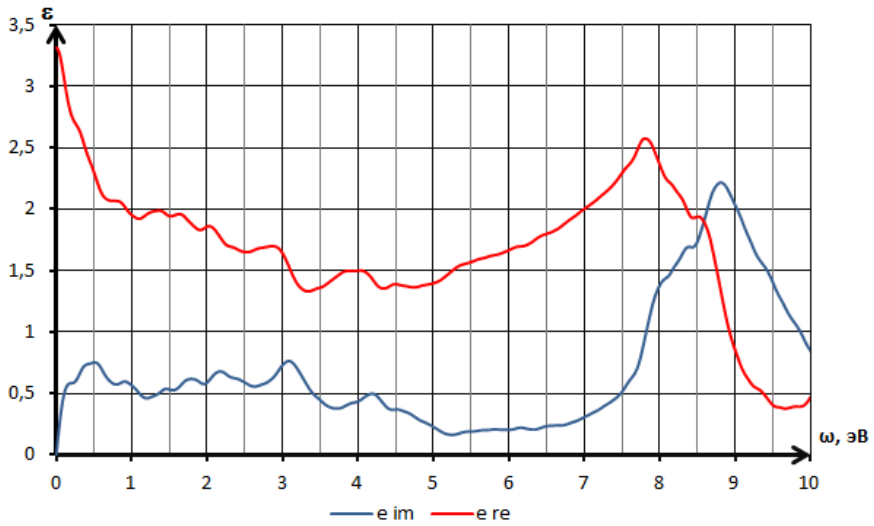

Fig. 5. Frequency dependence of the permittivity: imaginary (im) and real (re) constituents (WSe_2/ graphene)

Optic properties of the heterostructure were also simulated. Dispersion, having no sharp characteristic peaks on the dependence of absorption coefficient on frequency, was observed in the entire infrared and visible light range. The peak is observed at 8.75 eV. Consequently, absorption increases in the region of the far ultraviolet (Fig. 6). The heterostructure is optically transparent across the entire frequency spectrum. The refractive index in the visible light range is in the range from 1.21 to 1.43.

Brewster's angle and the critical angle were calculated for both investigated structures in the visible light range; they are given in Table 1.

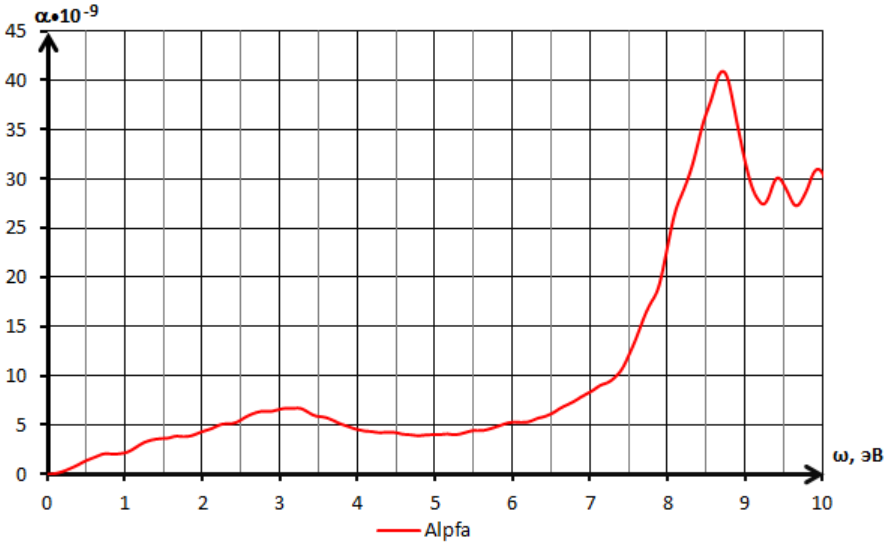

Fig. 6. Frequency dependence of the absorption coefficient (WSe_2/ graphene)

Table 1. Brewster's angle and the critical angle

Structure	Brewster's angle, degree	Critical angle, degree
MoS_2 / graphene	50.45 – 54.09	46.46 –50.46
WSe_2 / graphene	49.98 – 54.87	44.79 –57.21

The incidence angle, at which light reflected from a surface is perfectly polarized, is in the range from 50.45 to 54.09 for 2 / graphene heterostructure, and in the range from 49.98 to 54.87 for WSe2 / graphene heterostructure. The total internal reflection occurs in the ranges of 46.46-50.46 and 44.79 –57.21 for MoS_2 / graphene and WSe_2 / graphene heterostructures respectively.

4. Conclusions

Bilayered heterostructures of WSe_2/G and MoS_2/G have been theoretically simulated. Energy dispersion of graphene sheet in heterostructure has similar character to the pristine graphene. Vertical electric field (0.15 V/Å) weakly effects on the band gap WSe_2/G and MoS_2/G and can regulate charge transfer between monolayers and graphene. Utilization of Efield would lead to the realization of electronic properties engineering of the materials. A quantum-mechanical simulation was performed to determine the dielectric permittivity for a heterostructures. The peak in the dispersion of the absorption coefficient is observed at 8.5 eV for graphene monolayer and MoS_2 and at 8.75 eV for second heterostructure. The refractive index in the visible light range is in the range from 1.12 to 1.5 for investigated structures. Angle of incidence at which light that is reflected from the surface is perfectly polarized is in range from 50.45 to 54.09 for MoS_2 / graphene heterostructure, and is in range from 49.98 – 54.87 for WSe_2 / graphene heterostructure. The total internal reflection occurs can be observed in ranges from 46.46-50.46 and 44.79 –57.21 for MoS_2 / graphene and WSe_2 / graphene heterostructures respectively.

Acknowledgments. *This work was supported by the grants 2.53 of Belarusian National Scientific Research Program "Physical Materials Science, Novel Materials and Technologies" and 3.02 Belarusian National Scientific Research Program "Convergence 2020".*

References

[1] K.S. Novoselov, A.K. Geim, S.V. Morozov, D. Jiang, Y. Zhang, S.V. Dubonos, A.A. Firsov, Electric field effect in atomically thin carbon films // *Science* **306** (2007) 666.
[2] Y.W. Son, M.L. Cohen, S.G. Louie, Energy gaps in graphene nanoribbons // *Phys. Rev. Lett*. **97** (2006) 216803.
[3] A. Ebnonnasir, A. Narayanan, S. Kodambaka, C.V. Ciobanu, Tunable MoS_2 bandgap in MoS_2-graphene heterostructures // *Appl. Phys. Lett*. **105** (2014) 031603.
[4] U. Monteverde, J. Pal, M.A. Migliorato, M. Missous, U. Bangert, R. Zan, R. Kashtiban, D. Powell, Under pressure: control of strain, phonons and bandgap opening in rippled graphene // *Carbon* **91** (2015) 266.
[5] K. Kanayama, K. Nagashio, Gap state analysis in electric-field-induced band gap for bilayer graphene // *Scientific Reports* **5** (2015) 15789.
[6] K.F. Mak, C. Lee, J. Hone, J. Shan, T.F. Heinz, Atomically thin MoS_2: a new direct-gap semiconductor // *Phys. Rev. Lett*. **105** (2010) 136805.
[7] L. Britnell, R.M. Ribeiro, A. Eckmann, R. Jalil, B.D. Belle, A. Mishchenko, Y.J. Kim, R.V. Gorbachev, T. Georgiou, S.V. Morozov, A.N. Grigorenko, A.K. Geim, C. Casiraghi, A.H.C. Neto, K.S. Novoselov, Strong light-matter interactions in heterostructures of atomically thin films // *Science* **340** (2013) 1311.

[8] L.C. Upadhyay, J.J. Loferski, A. Wold, W. Giriat, R. Kershaw, Semiconducting properties of single crystals of n and p-type tungsten diselenide (WSe_2) // *J. Appl. Phys*. **39** (1968) 4736.
[9] H.L. Zeng, G.B. Liu, J.F. Dai, Y.J. Yan, B.R. Zhu, R.C. He, L. Xie, S.J. Xu, X.H. Chen, W. Yao, Optical signature of symmetry variations and spin3 valley coupling in atomically thin tungsten dichalcogenides // *Sci. Rep*. **3** (2013) 1608.
[10] C. Wul, F. Wang, C. Cai, Z. Xu, Y. Ma, F. Huang, F. Jia, M. Wang, Integration of graphene/ZnS nanowire film hybrid based photodetector arrays for high-performance image sensors // *2D Materials* **4(2)** (2017) 025113.
[11] G. Kresse, D. Joubert, From ultrasoft pseudopotentials to the projector augmented-wave method *// Phys. Rev. B: Condens. Matter Mater. Phys*. **59** (1999) 1758.
[12] G. Kresse, J. Furthmüller, Efficiency of ab-initio total energy calculations for metals and semiconductors using a plane-wave basis set // *Comput. Mater. Sci*. **6** (1996) 15.
[13] J.P. Perdew, K. Burke, M. Ernzerhof, Generalized gradient approximation made simple // *Phys. Rev. Lett*. **77** (1996) 3865.
[14] H.J. Monkhorst, J.D. Pack, Special points for Brillouin-zone integrations // *Phys. Rev. B: Condens. Matter Mater. Phys.* **13** (1976) 5188.
[15] I.V. Antonova, Vertical heterostructures based on graphene and other monolayer materials // *Phys. Semicond*. **50(1)** (2016) 67.
[16] P.E. Blöchl, Projector augmented-wave method *// Phys. Rev. B: Condens. Matter Mater. Phys.* **50** (1994) 17953.
[17] S. Grimme, J. Antony, S. Ehrlich, H. Krieg, A consistent and accurate ab initio parametrization of density functional dispersion correction (DFT-D) for the 94 elements H-Pu // *J. Chem. Phys*. **132** (2010) 154104.
[18] K. Momma, F. Izumi, VESTA 3 for three-dimensional visualization of crystal, volumetric and morphology data // *J. Mineral Petrol Sci*. **39** (2010) 136.